The Astrophysical Journal, 896:138 (5pp), 2020 June 20 https://doi.org/10.3847/1538-4357/ab91b4

Cosmic Evolution of Stellar-mass Black Hole Merger Rate in Active Galactic Nuclei

Y. Yang[1], I. Bartos[1], Z. Haiman[2], B. Kocsis[3], S. Márka[4], and H. Tagawa[5]
[1] Department of Physics, University of Florida, P.O. Box 118440, Gainesville, FL 32611-8440, USA; imrebartos@ufl.edu
[2] Department of Astronomy, Columbia University in the City of New York, 550 W 120th St., New York, NY 10027, USA
[3] Eötvös University, Institute of Physics, Pázmány P.s. 1/A, Budapest, 1117, Hungary
[4] Department of Physics, Columbia University in the City of New York, 550 W 120th St., New York, NY 10027, USA
[5] Institute of Physics, Eötvös University, Pázmány P.s., Budapest, 1117, Hungary
Received 2020 March 19; revised 2020 April 27; accepted 2020 May 8; published 2020 June 22

Abstract

Binary black hole mergers encode information about their environment and the astrophysical processes that led to their formation. Measuring the redshift dependence of their merger rate will help probe the formation and evolution of galaxies and the evolution of the star formation rate. Here we compute the cosmic evolution of the merger rate for stellar-mass binaries in the disks of active galactic nuclei (AGNs). We focus on recent evolution out to redshift $z = 2$, covering the accessible range of current Earth-based gravitational-wave observatories. On this scale, the AGN population density is the main contributor to redshift dependence. We find that the AGN-assisted merger rate varies by less than a factor of two in the range $0 < z \leqslant 2$, comparable to the expected level of evolution for globular clusters, but much smaller than the order-of-magnitude evolution for field binaries.

Unified Astronomy Thesaurus concepts: Gravitational wave astronomy (675); Active galactic nuclei (16)

1. Introduction

Observations by the LIGO and Virgo gravitational-wave detectors (Acernese et al. 2014; Aasi et al. 2015) show a high rate of stellar-mass black hole mergers of $\sim$10–100 Gpc^{-3} yr^{-1} (Abbott et al. 2019a). Despite the rapidly growing number of detections, however, the origin of these black hole mergers is currently not known. Possible formation mechanisms include isolated stellar binary evolution (Dominik et al. 2012; Kinugawa et al. 2014; Giacobbo et al. 2018; Bavera et al. 2019) and chance encounters in dense stellar clusters such as galactic nuclei or globular clusters (Portegies Zwart & McMillan 2000; O'Leary et al. 2006; Samsing et al. 2014; Rodriguez et al. 2015; O'Leary et al. 2016; Zhang et al. 2019).

Active galactic nuclei (AGNs) represent a unique environment in which the interaction of a dense cusp of stellar-mass black holes near the galactic center (Hailey et al. 2018) and the dense AGN accretion disk result in dramatically altered merger rates and properties (McKernan et al. 2014; Bartos et al. 2017b; Stone et al. 2017). As black holes orbiting the central, supermassive black hole cross the AGN disk, they experience friction that can align their orbit with the disk (Bartos et al. 2017b). Additional black holes can be born within the AGN disk due to gravitational fragmentation (Stone et al. 2017). Once in the disk, black holes migrate inward where their density further increases, enabling a higher rate of interaction (Tagawa et al. 2019).

AGN disks act as black hole assembly lines that collect and concentrate black holes in small volumes, enhancing their merger rate. The resulting rate can be a significant fraction of the total merger rate observed by LIGO and Virgo with estimates ranging within $\sim 10^{-3}$–10^{2} Gpc^{-3} yr^{-1} (McKernan et al. 2018, 2020; Tagawa et al. 2019; Yang et al. 2019b).

The properties of black holes within AGN-assisted mergers are expected to be different from other formation channels, enabling observational probes. Heavier black holes will be overrepresented in mergers within AGN disks compared to the black hole initial mass function (IMF) as they can more efficiently align their orbit with the disk (Yang et al. 2019b). In addition, as multiple black holes are driven toward the same small volume within the disk, consecutive mergers of the same black hole, or so-called hierarchical mergers, are common (Yang et al. 2019a). Such hierarchical mergers will result in characteristic high black hole spins, which will typically be aligned or antialigned with the binary orbit (Tagawa et al. 2019; Yang et al. 2019a). Two particular black hole mergers recorded by LIGO-Virgo so far, GW170729 (Abbott et al. 2019a) and GW170817A (Zackay et al. 2019), have the characteristically high mass and aligned spin expected from hierarchical mergers in AGN disks, albeit they are also consistent with other hierarchical formation channels (Yang et al. 2019a; Gayathri et al. 2020). Additional heavy black hole candidates have been reported that could have also originated from this channel and will require further investigation (Udall et al. 2019; Nitz et al. 2020).

Beyond the properties of the black holes themselves, AGNs provide other means to probe this population. Mergers in AGN disks are only expected in galaxies with active nuclei, which can be used to statistically differentiate them from other formation channels (Bartos et al. 2017a). Additionally, merger in a gas-rich environment may produce detectable electromagnetic emission (Bartos et al. 2017b; McKernan et al. 2019; Yi & Cheng 2019).

Here we investigated a distinct property of a binary merger population: its rate evolution with redshift. Redshift dependence can be used to differentiate between different formation channels and to better understand the underlying mechanisms that result in binary formation and merger. While the binary merger rate's redshift dependence has been previously explored for different binary formation scenarios (e.g., Fishbach et al. 2018), our analysis is the first such investigation for the AGN channel.

The paper is organized as follows. In Section 2 we examine the expected redshift evolution for different formation channels. In Section 3 we discuss the conversion of rate densities to detection rates. In Section 4 we present our results. We conclude in Section 5.

2. Binary Formation Channels

In this section we compute the expected cosmic evolution of the black hole merger rate density for the AGN channel, and review the expected evolution for field binaries and globular clusters from the literature.

2.1. The AGN Channel

The black hole merger rate in AGNs is proportional to the AGN population density $n_{\rm AGN}(z)$, where z is redshift. It can be evaluated through the AGN luminosity function (LF) $\phi_{\rm L}(L, z)$, which is a function of redshift and AGN luminosity L. The bolometric AGN LF can be fitted as (Shen et al. 2020):

$$\phi_{\rm L}(L, z) = \frac{\phi_*(z)}{\left[\frac{L}{L_*(z)}\right]^{\gamma_1(z)} + \left[\frac{L}{L_*(z)}\right]^{\gamma_2(z)}} {\rm Mpc}^{-3}, \quad (1)$$

where

$$\gamma_1(z) = a_0 T_0(1+z) + a_1 T_1(1+z) + a_2 T_2(1+z) \quad (2)$$

$$\gamma_2(z) = \frac{2b_0}{\left(\frac{1+z}{3}\right)^{b_1} + \left(\frac{1+z}{3}\right)^{b_2}} \quad (3)$$

$$\log Ł_*(z) = \frac{2c_0}{\left(\frac{1+z}{3}\right)^{c_1} + \left(\frac{1+z}{3}\right)^{c_2}} \quad (4)$$

$$\log \phi_*(z) = d_0 T_0(1+z) + d_1 T_1(1+z), \quad (5)$$

where T_n is the nth order Chebyshev polynomial. The best fit for the 11 parameters in this model are $\{a_0, a_1, a_2; b_0, b_1, b_2; c_0, c_1, c_2; d_0, d_1\} = \{0.8396, -0.2519, 0.0198; 2.5432, -1.0528, 1.1284; 13.0124, -0.5777, 0.4545; -3.5148, -0.4045\}$.

The direct integration of $\phi_{\rm L}(L, z)$ will yield the AGN density $n_{\rm AGN}(z)$. However, the lower end of the LF is subject to large uncertainty, thus we introduced a cutoff $L_{\rm min}$ when integrating. On the other hand, the mass of SMBHs can be correlated with the AGN luminosity via:

$$\frac{M_\bullet}{M_\odot} = 3.17 \times 10^{-5} \frac{1-\epsilon}{\dot{m}} \frac{L}{L_\odot}, \quad (6)$$

where ϵ is the radiation efficiency of the SMBH, $\dot{m} = \dot{M}_\bullet / \dot{M}_{\rm Edd}$, $\dot{M}_\bullet$ is the accretion rate of the SMBH, and $\dot{M}_{\rm Edd} = L_{\rm Edd}/\epsilon c^2$ is the Eddington rate.

Equation (6) could be rewritten to give a relation between the normalized accretion rate $\dot{m}$ and Eddington ratio $\lambda = L/L_{\rm Edd}$:

$$\dot{m} = (1-\epsilon)\lambda. \quad (7)$$

The Eddington ratio λ is found to take the form (Tucci & Volonteri 2017):

$$P(\lambda|L, z) = f_{\rm uno} P_1(\lambda|z) + f_{\rm obs} P_2(\lambda|z), \quad (8)$$

where $f_{\rm uno} = 1 - f_{\rm obs}$ is the fraction of unobscured (type-1) AGN and $f_{\rm obs}$ is the fraction of obscured (type-2) AGN. P_1 and P_2 are the Eddington ratio distributions of type-1 and type-2 AGNs, respectively.

$P_1(\lambda|z)$ follows a log-normal distribution:

$$P_1(\lambda|z) = \frac{1}{2\pi\sigma(z)\lambda} e^{-[\ln\lambda - \ln\lambda_{\rm c}(z)]^2/2\sigma^2(z)}, \quad (9)$$

with $\log\lambda_{\rm c}(z) = \max(-1.9 + 0.45z, \log(0.03))$ and $\sigma(z) = \max(1.03 - 0.15z, 0.6)$.

$P_2(\lambda|z)$ follows a gamma distribution with a cutoff at low-Eddington luminosities:

$$P_2(\lambda|z) = N_2(z)\lambda^{\alpha(z)} e^{-\lambda/\lambda_0}, \quad (10)$$

where $\lambda_0 = 1.5$ and $N_2(z)$ is the normalization factor. The slope of the power-law part, $\alpha(z)$, takes the form:

$$\alpha(z) = \begin{cases} -0.6 & z < 0.6 \\ -0.6/(0.4+z) & z \geqslant 0.6. \end{cases} \quad (11)$$

We assume that the Eddington ratio distribution has a cutoff ($\lambda_{\rm l}$) at low-Eddington luminosities, which is fixed to be 10^{-4} in our study. Our results below are not sensitive to this choice, which we confirmed for the $\lambda_{\rm l} = 10^{-4}$–$10^{-2}$ range.

The fraction $f_{\rm obs}$ can be parameterized as a function of X-ray luminosity $L_{\rm X}$ and redshift (Ueda et al. 2014):

$$f_{\rm obs} = \frac{(1+f_{\rm CTK})\psi(L_{\rm X}, z)}{1 + f_{\rm CTK}\psi(L_{\rm X}, z)}, \quad (12)$$

where $f_{\rm CTK}$ is the relative number density of compton thick (CTK, $\log N_{\rm H} > 24$) AGNs to that of compton thin (CTN, $\log N_{\rm H} = 20$–24) AGNs, $N_{\rm H}$ is the neutral hydrogen column density in unit of cm^{-2}. We assume $f_{\rm CTK} = 1$ is this work. ψ is the fraction of obscured AGNs ($\log N_{\rm H} = 20$–22) in total CTN AGNs and can be expressed as:

$$\psi(L_{\rm X}, z) = \min(\psi_{\rm max}, \max(\psi_{43.75}(z) - \beta(\log L_{\rm X} - 43.75), \psi_{\rm min})), \quad (13)$$

where we adopt $\psi_{\rm max} = 0.84$, $\psi_{\rm min} = 0.2$, and $\beta = 0.24$. $\psi_{43.75}(z)$ can be written as:

$$\psi_{43.75}(z) = \begin{cases} 0.43(1+z)^{0.48} & z < 2 \\ 0.43(1+2)^{0.48} & z \geqslant 2. \end{cases} \quad (14)$$

Since $f_{\rm obs}$ is dependent on X-ray luminosity, we need to convert the bolometric luminosity to the X-ray luminosity using a bolometric correction (Marconi et al. 2004):

$$\log(L/L_{\rm X}) = 1.54 + 0.24\xi + 0.012\xi^2 - 0.0015\xi^3, \quad (15)$$

with $\xi = \log L/L_\odot - 12$. lower limit of the Eddington ratio. The distribution function of λ is independent of the redshift; therefore, the average Eddington ratio is a constant for $z \lesssim 1$, as shown by other studies (Georgakakis et al. 2017).

We additionally need the BH merger rate (Γ) of a single AGN. Yang et al. (2019b) showed that several factors affect the BH merger rate, of which $\dot{m}$ is the dominant one. We assumed that the mean number ($N_{\rm disk}$) of stellar black holes in the AGN disk is a univariate function of $\dot{m}$ and obtained a power-law fit ($M_\bullet = 10^6 M_\odot$, $\epsilon = 0.1$):

$$N_{\rm disk}(\dot{m}) = 5.5\,\dot{m}^{1/3}. \quad (16)$$

We assume that the black holes in AGN disks will hierarchically merge in the migration traps (Yang et al. 2019a) and the number of stellar black holes in AGN disks follows a Poisson distribution with a mean value of $N_{\rm disk}$. Consequently, the average BH merger rate is:

$$\Gamma(\dot{m}) = (N_{\rm disk}(\dot{m}) - 1 + e^{-N_{\rm disk}(\dot{m})})/\tau_{\rm AGN}, \quad (17)$$

where $\tau_{\rm AGN} = 10^7$ yr is the AGN lifetime.

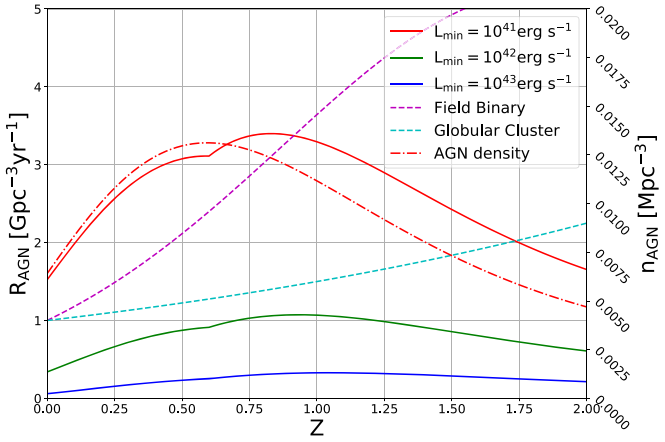

Figure 1. Cosmic AGN-assisted black hole merger rate as a function of redshift for several choices of $L_{\rm min}$. We adopted a radiation efficiency of $\epsilon = 0.1$. We compared their merger rate with the merger rate (dashed lines) of BBHs from globular clusters and field binaries, whose local merger rate at $z = 0$ is fixed to be 1 Gpc^{-3} yr^{-1}. We also added the AGN density distribution (dotted dashed line) with $L_{\rm min} = 10^{41}$ erg s^{-1}.

We note that this dependence is different for several subdominant merger processes associated with AGNs (see Tagawa et al. 2019 for a comparison of different contributing processes); however, we found that our results below only weakly depend on the specific form of $\Gamma(\dot{m})$. Therefore, other AGN-related processes will not alter our results below.

Combining these above factors, we arrived at an expression for the redshift-dependence of the cosmic BH merger rate in AGN:

$$R_{\rm AGN}(z) = \int_{L\in I_{\rm L}} \phi_{\rm L} d\log L \int_{\lambda_{\rm l}}^{1} \Gamma(\dot{m}) P(\lambda|L, z) d\lambda. \quad (18)$$

Here, the integral domain of the luminosity is $I_{\rm L} = [L_{\rm min}, 3.15 \times 10^{14} L_{\odot}]$.

We show $R_{\rm AGN}(z)$ in Figure 1 for multiple choices of $L_{\rm min}$. We see that the distribution only weakly depends on z, with a maximum around $z = 0.8$ which is about a factor of two greater than the minimum at $z = 0$. We also see that the choice of Ł$_{\rm min}$ does not meaningfully affect the normalized redshift distribution of $R_{\rm AGN}(z)$, although it does change the magnitude of merger rate density. Therefore, in the following, we adopted $L_{\rm min} = 10^{41}$ erg s^{-1} as our fiducial model.

2.2. Field Binaries

We also compared our model with other formation channels. The first considered mechanism is the field binary channel. We assumed that the formation rate density of field binaries in comoving volume follows the low-metallicity star formation rate (SFR; Fishbach et al. 2018):

$$\rho_{\rm FB}(z) \propto \psi_{\rm MD}(z) f_{\rm Z}(z) \propto \frac{(1+z)^{2.7}}{1+\left(\frac{1+z}{2.9}\right)^{5.6}} \gamma\left(0.84, \left(\frac{Z}{Z_{\odot}}\right)^2 10^{0.3z}\right), \quad (19)$$

where $\psi_{\rm MD}(z)$ is the Madau–Dickinson SFR (Madau & Dickinson 2014) and $f_{\rm Z}(z)$ is the fraction of star formation occurring at metallicity smaller than Z, $\gamma(s, x)$ is the lower incomplete gamma function.

Since the binaries do not merge immediately after their formation, we adopted a time-delay model to estimate the merger rate density:

$$R_{\rm FB} = \int_{z_{\rm m}}^{\infty} \rho_{\rm FB}(z_{\rm f}) p(t(z_{\rm f}) - t(z_{\rm m})) \frac{dt}{dz_{\rm f}} dz_{\rm f}, \quad (20)$$

where $p(t)$ is the distribution of time delay and $t(z)$ is the cosmological look back time. We assumed that the time delay had a flat distribution in log space between 50 Myr and 15 Gyr. The mass distribution was assumed to be (Fishbach et al. 2018):

$$f_{\rm FB}(m_1, m_2) = \frac{1-\alpha}{M_{\rm max}^{1-\alpha} - (5M_{\odot})^{1-\alpha}} \frac{m_1^{-\alpha}}{m_1 - 5M_{\odot}}, \quad (21)$$

where $5M_{\odot} < m_2 < m_1 < M_{\rm max}$.

2.3. Globular Clusters

Another channel we considered is the dynamical formation in globular clusters (e.g., Fragione & Kocsis 2018). We found that the merger rate density at $z \lesssim 2$ can be parameterized as $R_{\rm GC} = 18.6 \times \left(\frac{3}{2}\right)^z$ Gpc^{-3} yr^{-1}. We also considered other merger rate density distribution (e.g., Rodriguez et al. 2016; Rodriguez & Loeb 2018), but it does not change at $z \lesssim 2$ by more than a factor of 3. Thus, we adopted the exponential parameterization in our analysis. The mass function was assumed to be the same as above.

3. Conversion to Detection Rate

In order to compare the expected redshift evolutions to black hole merger observations via gravitational waves, we need to convert the expected merger rate distribution $R_{\rm merger}$ to detection rate distribution $R_{\rm det}$ using the sensitive distance range of LIGO-Virgo.

$$R_{\rm det}(z) = \frac{R_{\rm merger}}{1+z} \frac{dV_{\rm c}}{dz} \int P_{\rm det}(\mathcal{M}) f(m_1, m_2) dm_1 dm_2. \quad (22)$$

Here, $V_{\rm c}$ is the comoving volume and $f(m_1, m_2)$ is the mass function of binary black holes in AGN disks. $P_{\rm det}(\mathcal{M})$ is the probability of an event at redshift z with detector-frame chirp mass

$$\mathcal{M} = (1+z) \frac{(m_1 m_2)^{3/5}}{(m_1+m_2)^{1/5}} \quad (23)$$

being detected by advanced LIGO. In our calculations, we assumed that an event is detectable when its signal-to-noise ratio (S/N) is greater than 8. The S/N of a black hole merger is (O'Shaughnessy et al. 2010):

$$\rho = 8\omega \frac{370\ {\rm Mpc}}{D_{\rm L}(z)} \left(\frac{\mathcal{M}}{M_{\odot}}\right)^{5/6}, \quad (24)$$

where $D_{\rm L}(z)$ is the luminosity distance corresponding to redshift z, and $\omega \in [0, 1]$ is a geometrical factor determined by the position and orientation of the binary system.[6] We adopt the noise power spectral density of LIGO at its design

[6] The tabular data of $P(\omega)$ can be found online at http://www.phy.olemiss.edu/~berti/research.html.

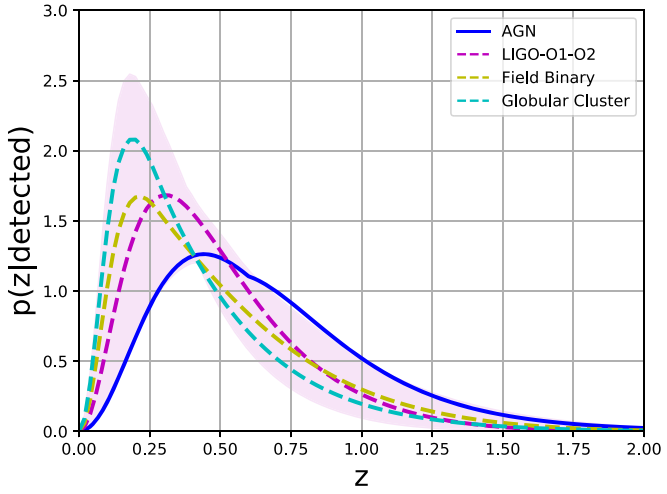

Figure 2. Expected redshift distribution of detected gravitational wave events by Advanced LIGO-Virgo at design sensitivity. The fitted parameters of the model for LIGO's detections (LIGO-O1-O2) are $m_{\rm min} = 7.8M_{\odot}$, $m_{\rm max} = 40.8M_{\odot}$, $\alpha = 1.3$, $\beta_{\rm q} = 6.9$, and the shaded region is the 90% credible intervals (Abbott et al. 2019b). For the field binary channel, we assume that the formation rate density of field binaries follows the low-metallicity star formation rate and adopt a time-delay model to evaluate the merger rate density. For the dynamical mergers in the globular cluster, we postulate the merger rate density $R_{\rm GC} \propto (3/2)^z$.

sensitivity (Ajith 2011; Martynov et al. 2016) in the evaluation of the S/N above.

Yang et al. (2019b) found that the AGN disk can significantly change the IMF of merging black holes. The hierarchical black hole mergers will then alter the mass distribution of binary black holes (Yang et al. 2019a) since the mass of one component (the remnant of the previous merger) of the binary will increase as the hierarchical merging process continues. We adopted the weighted average binary mass distribution in their work($N_{\rm disk} = 2.5$):

$$\bar{f}\,(m_1, m_2) = \sum_{\rm n=1}^{\infty} P_{\rm n} f_{\rm n}\,(m_1, m_2), \tag{25}$$

where $P_{\rm n}$ and $f_{\rm n}$ are the fraction and mass distribution of nth generation, respectively.

4. Results

We calculated the expected redshift distributions of detected events for the models described in Section 2 using the conversion described in Section 3. We then compared these distributions to the reconstructed cosmic evolution for black hole mergers observed through gravitational waves by LIGO-Virgo during the O1 and O2 observing periods (Model B in Abbott et al. 2019b).

Our results are shown in Figure 2. We see that the expected rate evolution for LIGO-Virgo observations is currently uncertain and is essentially consistent with all three formation channel models considered here. Looking at the LIGO-Virgo distribution using its expected value, we see that the observed distribution peaks at a higher redshift than the field-binary and globular cluster channels, but at a lower redshift than our AGN model. Taking this expected distribution at face value, the observed distribution is consistent with the linear combination of an AGN and a field-binary population, with 40% and 60% contributions, respectively.

A more precise determination of the binaries' origin can be done through the more accurate measurement of their redshift evolution. Current uncertainty on the measured evolution includes all three models considered here. However, looking at Figure 2, we see that the AGN channel falls on the lowest end of this uncertainty region, while field binaries and globular clusters are at the very high end. Therefore, even a modest improvement on the precision of cosmic evolution should be able to rule out either AGNs or the other two channels as the sole origin of the observed binaries. Additionally, for differentiating between formation channels, other information will be useful, such as black hole masses, spins, and host galaxies. We therefore anticipate that with the rapid increase in the number of detections, differentiation between formation channels on the population level will be possible soon.

5. Conclusion

We computed the expected redshift distribution of the merger rate of stellar-mass black hole mergers in AGN disks. We found that the distribution is close to being uniform out to $z \approx 1$, which is distinct from our expectations for field binaries and for some other dynamical merger scenarios, such as in globular clusters. This distinct evolution, together with other differences, can help differentiate between the possible origins of binary mergers and help probe their environment.

The authors are thankful to the University of Florida and Columbia University in the City of New York for their generous support. The Columbia Experimental Gravity group is grateful for the generous support of the National Science Foundation under grant PHY-1708028. This project was supported by funds from the European Research Council (ERC) under the European Union's Horizon 2020 research and innovation program under grant agreement No. 638435 (GalNUC) and by the Hungarian National Research, Development, and Innovation Office grant NKFIH KH-125675 (to B.K. and H.T.). Z.H. acknowledges support from NASA grant NNX15AB19G and NSF grant 1715661.

ORCID iDs

I. Bartos https://orcid.org/0000-0001-5607-3637
Z. Haiman https://orcid.org/0000-0003-3633-5403
B. Kocsis https://orcid.org/0000-0002-4865-7517

References

Aasi, J., Abbott, B. P., Abbott, R., et al. 2015, CQGra, 32, 074001
Abbott, B. P., Abbott, R., Abbott, T. D., et al. 2019a, PhRvX, 9, 031040
Abbott, B. P., Abbott, R., Abbott, T. D., et al. 2019b, ApJL, 882, L24
Acernese, F., Agathos, M., Agatsuma, K., et al. 2014, CQGra, 32, 024001
Ajith, P. 2011, PhRvD, 84, 084037
Bartos, I., Haiman, Z., Marka, Z., et al. 2017a, NatCo, 8, 831
Bartos, I., Kocsis, B., Haiman, Z., & Márka, S. 2017b, ApJ, 835, 165
Bavera, S. S., Fragos, T., Qin, Y., et al. 2019, A&A, 635, A97
Dominik, M., Belczynski, K., Fryer, C., et al. 2012, ApJ, 759, 52
Fishbach, M., Holz, D. E., & Farr, W. M. 2018, ApJL, 863, L41
Fragione, G., & Kocsis, B. 2018, PhRvL, 121, 161103
Gayathri, V., Bartos, I., Haiman, Z., et al. 2020, ApJL, 890, L20
Georgakakis, A., Aird, J., Schulze, A., et al. 2017, MNRAS, 471, 1976
Giacobbo, N., Mapelli, M., & Spera, M. 2018, MNRAS, 474, 2959
Hailey, C. J., Mori, K., Bauer, F. E., et al. 2018, Natur, 556, 70
Kinugawa, T., Inayoshi, K., Hotokezaka, K., Nakauchi, D., & Nakamura, T. 2014, MNRAS, 442, 2963
Madau, P., & Dickinson, M. 2014, ARA&A, 52, 415
Marconi, A., Risaliti, G., Gilli, R., et al. 2004, MNRAS, 351, 169

Martynov, D. V., Hall, E. D., Abbott, B. P., et al. 2016, PhRvD, 93, 112004
McKernan, B., Ford, K. E. S., Bartos, I., et al. 2019, ApJL, 884, L50
McKernan, B., Ford, K. E. S., Bellovary, J., et al. 2018, ApJ, 866, 66
McKernan, B., Ford, K. E. S., Kocsis, B., Lyra, W., & Winter, L. M. 2014, MNRAS, 441, 900
McKernan, B., Ford, K. E. S., & O'Shaughnessy, R. 2020, arXiv:2002.00046
Nitz, A. H., Dent, T., Davies, G. S., et al. 2020, ApJ, 891, 123
O'Leary, R. M., Meiron, Y., & Kocsis, B. 2016, ApJL, 824, L12
O'Leary, R. M., Rasio, F. A., Fregeau, J. M., Ivanova, N., & O'Shaughnessy, R. 2006, ApJ, 637, 937
O'Shaughnessy, R., Kalogera, V., & Belczynski, K. 2010, ApJ, 716, 615
Portegies Zwart, S. F., & McMillan, S. L. W. 2000, ApJL, 528, L17
Rodriguez, C. L., Chatterjee, S., & Rasio, F. A. 2016, PhRvD, 93, 084029
Rodriguez, C. L., & Loeb, A. 2018, ApJL, 866, L5
Rodriguez, C. L., Morscher, M., Pattabiraman, B., et al. 2015, PhRvL, 115, 051101
Samsing, J., MacLeod, M., & Ramirez-Ruiz, E. 2014, ApJ, 784, 71
Shen, X., Hopkins, P. F., Faucher-Giguère, C.-A., et al. 2020, arXiv:2001.02696
Stone, N. C., Metzger, B. D., & Haiman, Z. 2017, MNRAS, 464, 946
Tagawa, H., Haiman, Z., & Kocsis, B. 2019, arXiv:1912.08218
Tucci, M., & Volonteri, M. 2017, A&A, 600, A64
Udall, R., Jani, K., Lange, J., et al. 2019, arXiv:1912.10533
Ueda, Y., Akiyama, M., Hasinger, G., Miyaji, T., & Watson, M. G. 2014, ApJ, 786, 104
Yang, Y., Bartos, I., Gayathri, V., et al. 2019a, PhRvL, 123, 181101
Yang, Y., Bartos, I., Haiman, Z., et al. 2019b, ApJ, 876, 122
Yi, S.-X., & Cheng, K. S. 2019, ApJL, 884, L12
Zackay, B., Dai, L., Venumadhav, T., Roulet, J., & Zaldarriaga, M. 2019, arXiv:1910.09528
Zhang, F., Shao, L., & Zhu, W. 2019, ApJ, 877, 87